Recent Results from the NAL Bubble Chamber

J. C. Vander Velde*

The University of Michigan, Ann Arbor, Michigan 48104

ABSTRACT

We present a summary of results obtained during the last few months from the 30-inch hydrogen bubble chamber at National Accelerator Laboratory.

INTRODUCTION

We start by giving a table of pictures taken so far at NAL.

Table I. NAL Bubble Chamber Exposures (as of August, 1973)

P_{beam}	Exposure	Pictures In Hand	Groups
102	pp	30,000	Michigan - Rochester
205	pp	50,000	ANL - NAL - Stony Brook
303	pp	50,000	NAL - UCLA
405	pp	12,000	Michigan - Rochester
205	π^-p	50,000	LBL - NAL
205	pp HYBRID	16,000	ANL - Iowa St. - Maryland
303	pp HYBRID	18,000	Michigan State - NAL
100	$(\pi^+/p)p$(Tagged)	50,000	U. C. Davis

We want to emphasize that there are a lot of hard working people in all these groups and we are extremely grateful to them for providing us with the data we will present, most of which are unpublished as yet.

The broad topics we want to cover are as follows:

I. SLOW P SPECTRA (Diffractive Production)
II. σ_T, σ_{EL}, σ_n
III. PRODUCTION OF NEUTRALS
IV. CHARGE TRANSFER AND CORRELATIONS

I. SLOW PROTON SPECTRA

The "diffractive" peak in the proton spectrum was first seen at the ISR in 1972.[1] This was confirmed in the NAL bubble chamber at 100, 200 and 300 GeV and an estimate of 7 mb was made for the diffractive cross section. It was also seen that the phenomenon occured primarily in the 2 and 4 (charged) prong topologies at these energies.[2]

*Research supported in part by the U. S. Atomic Energy Commission

X and M^2 DEPENDENCE

Using the variables $X = 2 P_{\parallel}^{*} / \sqrt{S}$ and $M^2 \approx m_p^2 + S(1 - |X|)$ we show in Figure 1 the $d\sigma/dX$ distribution at 102 GeV for all inelastic events with a slow proton. By "slow" we mean $P_{lab} < 1.2$ GeV/c, such that they can be reliably identified by ionization. This P_{lab} cut causes a bias for $X \lesssim -.5$. (The invariant cross section $Ed^3\sigma/dP^3$ integrated over P_T^2 is approximately equal to $Xd\sigma/dX$.)

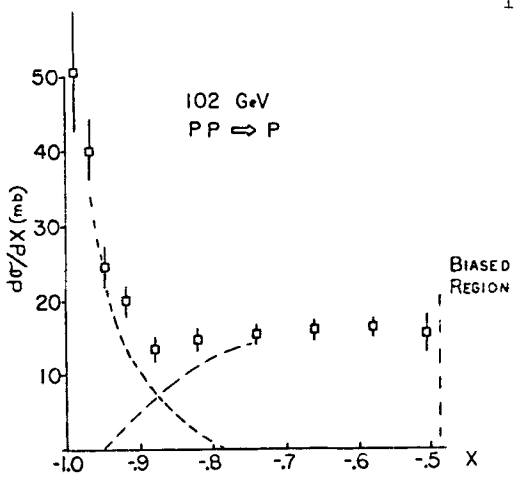

Fig.1. X distribution of slow protons.

One gets 6 - 7 mb for the diffractive peak ($|X| \gtrsim .9$) by estimating the shapes of the peak and background in the region where they overlap (dotted lines). (When quoting <u>total</u> diffractive cross sections we always multiply the observed cross section by 2 to account for pp symmetry.)

The fact that the diffractive component restricts itself to low prong numbers can be seen in Figure 2 where we show $d\sigma/dM^2 = (1/S)\, d\sigma/dX$ at 205 GeV. (The reader can use 4.35 μb/event to convert this Figure to cross section.)

Note the events at negative M^2 give an indication of the M^2 resolution due to angle errors on the short protons. This resolution in M^2 deteriorates proportional to P(beam).

There is evidence (not shown) that the higher prong numbers start to contribute more strongly to the peak as S increases. This agrees with the observation at the ISR of a clear diffractive peak for ≥ 6 prongs.

Similarly, in Figure 3, the new results from 205 GeV <u>$\pi^- p$</u> interactions are shown.

From this we conclude that

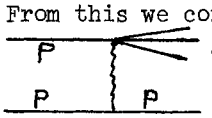

is remarkably similar to

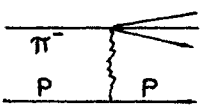

The LBL - NAL group estimates 2.3 ± .2 mb for the diffractive peak. Curiously enough, they also get ~ 2.4 mb for $\sigma_{EL}(\pi^- p)$ at 205 GeV. Hence $\pi^- p$ is like pp in this respect also; the diffractive inelastic cross section is of the same size as the elastic cross section in both cases.

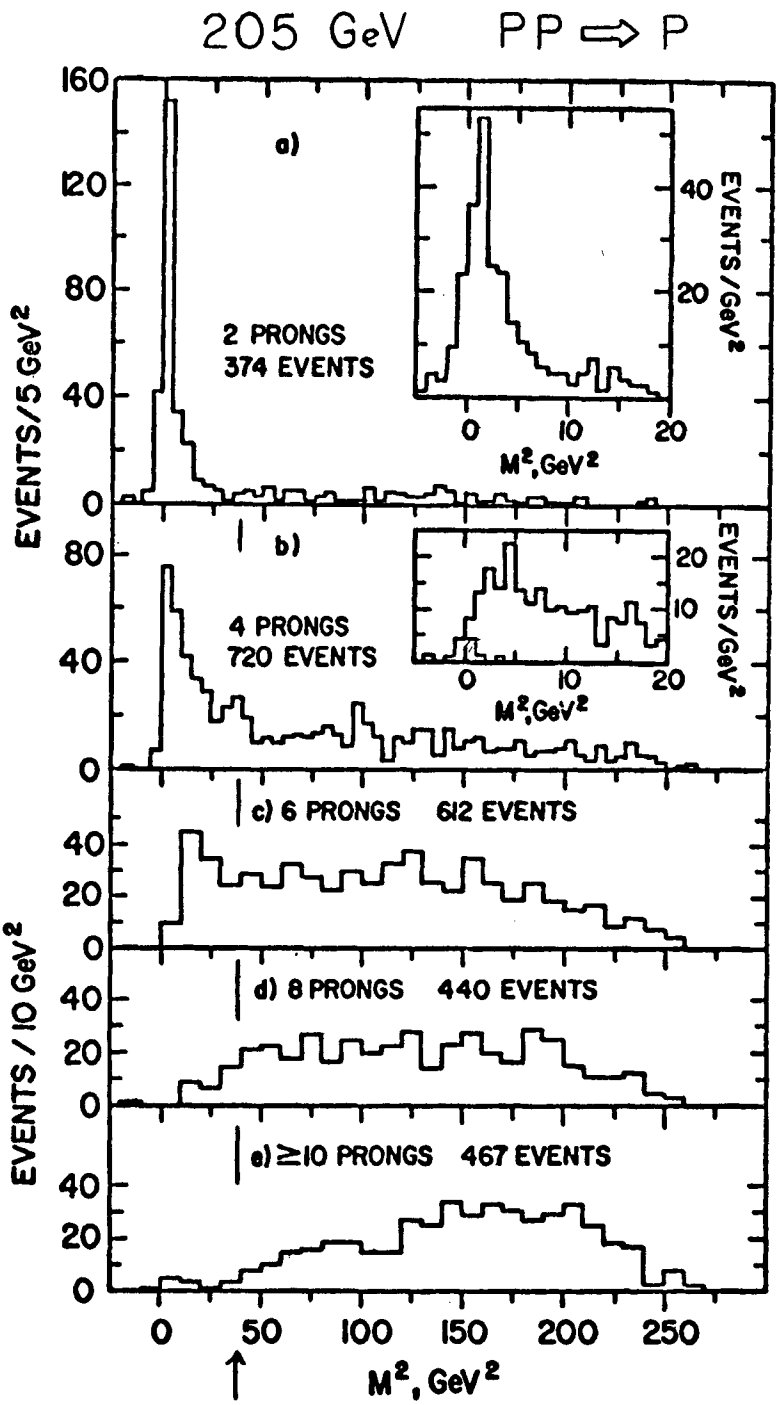

Fig.2. M^2 distribution for various topologies. The arrow marks X = -.9 at 205 GeV.

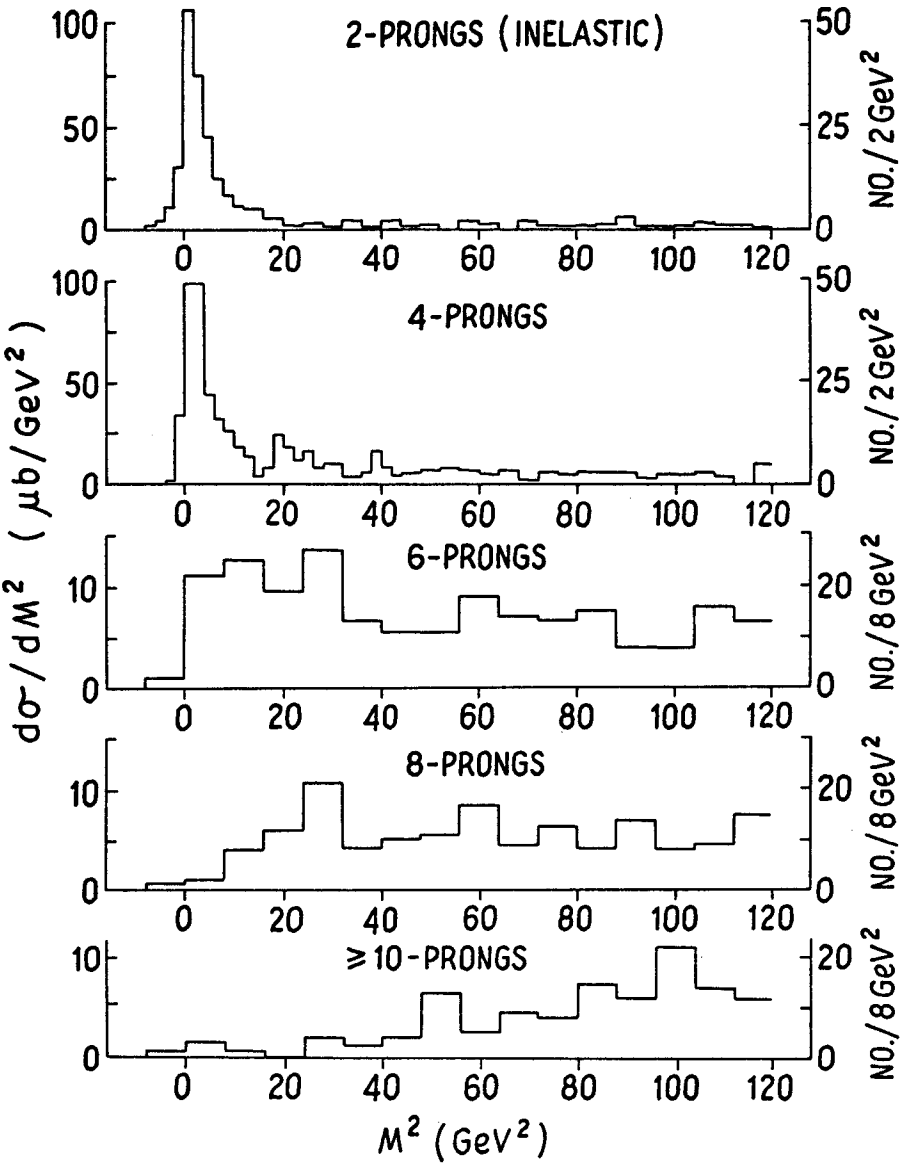

Fig.3. M^2 distribution for 205 GeV $\underline{\pi^- p}$ interactions.

DEPENDENCE ON S.

New results have just become available from 405 GeV pp interactions. The comparison of $d\sigma/dM^2$ at 405 GeV and 102 GeV is shown in Figure 4.

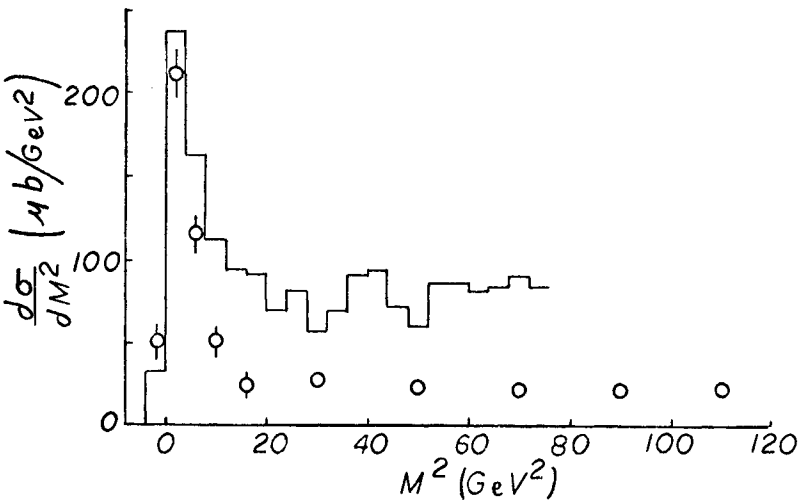

Fig.4. $d\sigma/dM^2$ for pp → p + M. Histogram is 102 GeV data, circles are 405 GeV data.

It is seen that the peak below $M^2 \approx 10$ remains approximately constant with energy, whereas the higher M^2 region falls approximately $\propto 1/P(\text{beam}) \propto 1/S$. We see this same behavior in the 4-prong events at 102, 205, and 405 GeV shown in Figure 5. The 400 GeV data shows a strikingly sharp peak for $M^2 < 10$ which was not as evident at 100 and 200 GeV. This $M^2 < 10$ peak appears to remain constant with energy whereas the $M^2 > 10$ region falls with energy.

From this we conclude the following:

(1) The region $M^2 < 10$ GeV^2 has the properties of good old fashioned Good-Walker diffraction dissociation; $d\sigma/dM^2$ is independent of S. For the 4 prong cross sections and $M^2 < 12$ we get

$$205 \text{ GeV}: \quad \sigma = (1.4 \pm .1) \text{ mb}$$
$$405 \text{ GeV}: \quad \sigma = (1.3 \pm .2) \text{ mb}$$

We will refer to this $M^2 < 10$ peak as the D_I component.

(2) Immediately above $M^2 \sim 10$ the cross section $d\sigma/dM^2$ at a

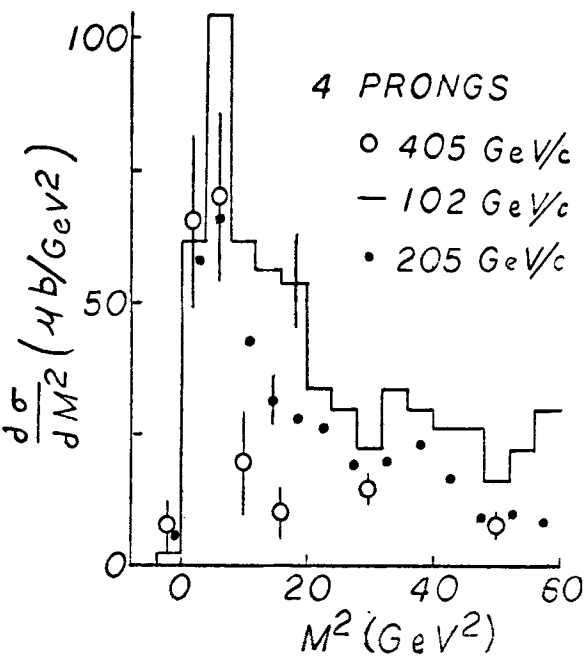

Fig.5. Comparison of the M^2 distribution for 4-prongs at three different energies.

given M^2 falls rapidly with S. This region cannot be the D_I component. It also cannot be due to the so-called triple Pomeron (PPP) term[3] which gives $d\sigma/dM^2 \propto 1/M^2$ and independent of S. (The 205 GeV researchers have shown that the $M^2 < 10$ peak is ~80% due to the 4-constraint final state $pp\pi^+\pi^-$, whereas the $10 < M^2 < 50$ region is predominantly due to events with extra neutrals produced.[4])

In order to investigate this further we plot $d\sigma/dX$ for these same 4-prong events in Figure 6. Here we see further evidence for three regions of behavior in the proton spectrum (from left to right):

(1) The region $-.9 < X < -.5$ ("broad hump") scales with S approximately. (It falls slightly due to the decrease in the total 4-prong cross section.)

(2) At $X \approx -.9$ the cross section at any S begins to rise, but at a given X it falls with S.

(3) For $M^2 < 10$ the cross section $d\sigma/dX$ at a given M^2 suddenly becomes proportional to S (all three curves cross !) in agreement with the D_I component behavior.

Region (2) ($X = -.9$ down to $M^2 = 10$) has a behavior which shows it is different from both the "broad hump" and the D_I ($M^2 < 10$) components. We call this the D_{II} component. It appears to have the following properties:

(a) At $|X| \sim .9$, $d\sigma/dX$ starts to rise above the broad hump at all energies (NAL, ISR). This is due to the D_{II} component.

(b) At a given X it increases its multiplicity rapidly with S. (At a fixed X, $M^2 \propto S$, and we know that $\langle n \rangle$ is a function only of M^2, thus $\langle n \rangle$ must increase with S.)[5]

(c) In the region $-.95 < x < -.90$ the cross section $d\sigma/dX$, as a function of S, appears to be falling slowly (not scaling) when summed over all topologies, as can be seen from the

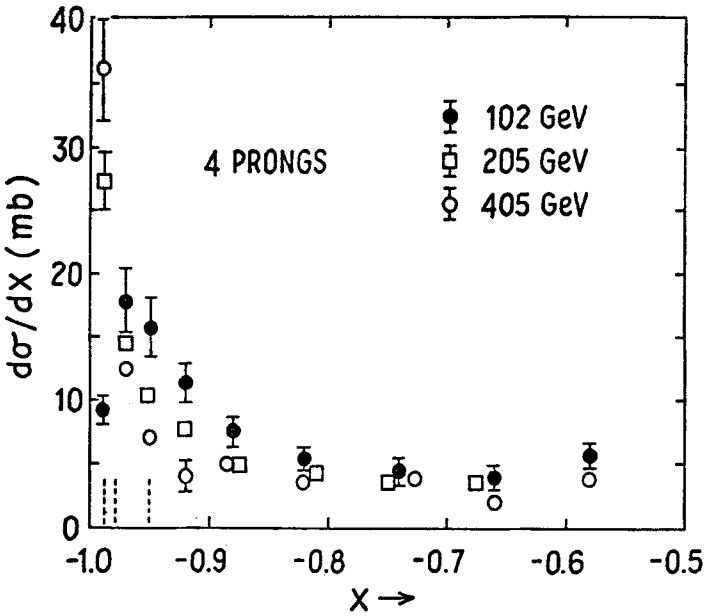

Fig.6. Comparison of the X distribution for 4-prongs at three different energies. The dotted lines mark the position of $M^2 = 10$ at each energy.

following table.

Table 2. Average dσ/dX (all inelastic) for $-.95 < X < -.90$

Beam Energy	$S(GeV^2)$	M^2 interval	$< d\sigma/dX >$ (mb)
102 GeV	196	$10.7 < M^2 < 20.5$	20 ± 2
205 GeV	386	$20.2 < M^2 < 39.5$	17 ± 1
405 GeV	762	$139.0 < M^2 < 77.0$	15 ± 2

(Due to uncertainties in the elastic contamination in 2-prong inelastic events it is not possible to obtain very accurate estimates of the total inelastic cross section for $-1.0 < x < -.9$. The best estimates we have at present are (3.0 ± .3) mb, (3.1 ± .3) mb, and (3.3 ± .4) mb at 102, 205, and 405 GeV respectively. Multiplying these numbers by 2 gives the total "diffractive" ($D_I + D_{II}$) cross section for $|X| > .9$. These events appear to be split about equally between the D_I ($M^2 < 10$) and D_{II} components, i.e., about 3 mb for each.)

The last column of Table 2 shows that there is a slow decrease of dσ/dX at a given X for the D_{II} component. On the other hand, there is a dramatic energy dependence for $d\sigma/dM^2$ in a given M^2 interval. It falls rapidly with S in the D_{II} region, as can be seen from Table 3.

Table 3. Average $d\sigma/dM^2$ (all inelastic) for $12 < M^2 < 30$

Beam Energy	X interval	$< d\sigma/dM^2 >$ ($\mu b/GeV^2$)
205 GeV	$-.971 < X < -.925$	58 ± 4
405 GeV	$-.985 < X < -.962$	25 ± 5

It is clear from Table 3 that the D_{II} region at NAL energies is not dominated by "triple Pomeron" behavior ($d\sigma/dM^2$ independent of S at a given M^2). This is further supported by Figure 4 where we see that the 400 GeV $d\sigma/dM^2$ does not fall like $1/M^2$ in the D_{II} region ($10 < M^2 < 77$).

SUMMARY

To summarize, I believe we have evidence for two different types of behavior in the "diffractive" ($|X| > .9$) region. The low mass (D_I) component ($M^2 < 10$ GeV^2) looks like old fashioned diffraction dissociation; $d\sigma/dM^2$ is independent of S. The high mass component (up to $|X| = .9$) is not like D_I. It also does not have the correct S and M^2 dependence to be triple Pomeron.

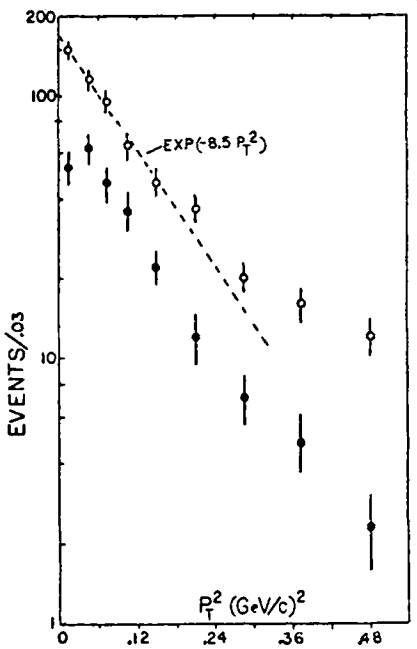

Fig.7. P_T^2 dependence of protons. o 102 and 405 GeV, ≥ 4 prongs, $-.9 < X < -.6$. ● 102, 205, 303, 405 GeV, 4 Prongs, $M^2 < 10$.

P_T^2 DEPENDENCE

In Figure 7 we show the P_T^2 dependence of the D_I region and the "broad hump" region. The broad hump has an early slope of ~ 8.5 and then flattens out. The D_{II} region (not shown) has a slope of ~ 7 with no evidence of a turnover. The D_I region shows some evidence for a turnover in 4-prongs at $P_T^2 \sim .04$. Beyond .05 the slope ~ 10. In the 205 GeV π^-p data there is no corresponding turnover for 4-prongs, $M^2 < 10$ (not shown).

II. TOTAL σ, ELASTIC σ, MULTIPLICITY

In Table 4 we compare cross sections at 100 and 400 GeV measured by the same group (Michigan-Rochester).

Table 4. Cross Sections at 100 and 400 GeV (mb).

P_{lab}	σ_{tot}	σ_{elas}	σ_{inel}	2 Pr. inel	≥ 4 Pr.
102	38.9±.8	7.0±.5	31.9±.7	4.5±.4	27.4±.6
405	40.6±1.1	7.8±.6	32.8±1.0	2.7±.5	30.1±.7
Δσ	1.7±1.4	.8±.8	.9±1.2	-1.8±.6	2.7±.9

We see some (statistically weak) evidence for a rise in both the elastic and inelastic cross sections. The higher multiplicities are clearly still rising rapidly. For ≥6 prongs we find $\Delta\sigma = (6.0 \pm .8)$ mb. It is not clear to me what this means, if anything, vis-a-vis the rise in σ_{tot} seen at the ISR.

MULTIPLICITY

In Figure 8 we show $< n^- >$, f_2^-, and f_3^- from bubble chamber inelastic data in the range 50 to 400 GeV.[20]

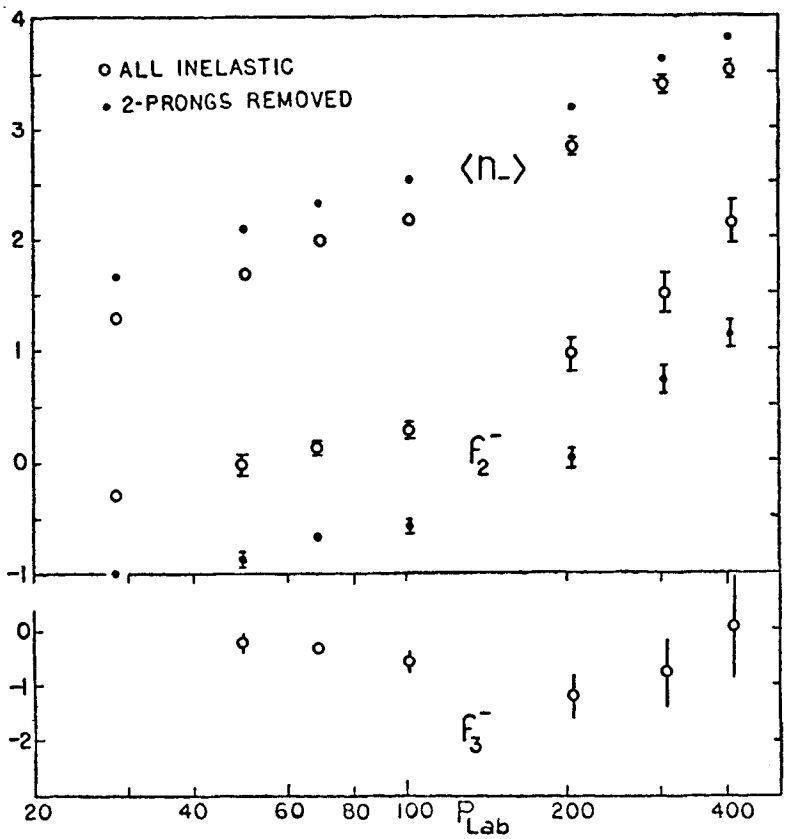

Fig. 8. Moments of the multiplicity distribution vs. beam momentum.

(1) $< n^- >$ gives a reasonably good fit to a straight line vs. ln S. However, if we take out the inelastic 2-prongs from the computation of $< n^- >$ we get what looks like a break in $< n^- >$ at about 100 GeV. (This removal reduces the errors considerably and provides a more reliable comparison between experiments.) We remark that the break at 100 GeV may be connected to the rise in the total cross section which starts at the same place.

(2) f_2^- apparently requires a $\ln^2 S$ term.

(3) f_3^- is consistent with going negative at high energies, which would be required by two-component models[6], but the trend above 200 GeV is for it to become positive.

It was observed at 100 GeV that taking out the D_I and D_{II} components leaves a multiplicity distribution for the remaining events (ND) which is very nearly Poisson.[7] This behavior, which also holds at 303 GeV[8], is shown in Figures 9 and 10. It is apparent that the ND component is becoming too wide at 400 GeV for this idea to work exactly. The D components in Figures 9 and 10 are defined by $|X| > .88$ and $|X| > .90$ respectively.

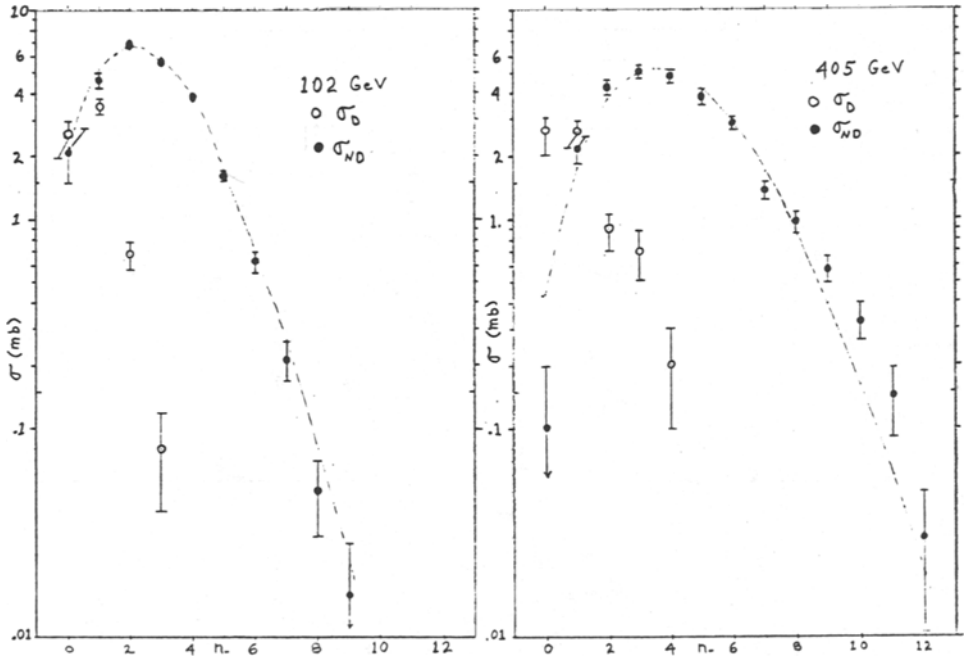

Figs. 9 and 10. Multiplicity distribution for D and ND components. The curves are Poissons with $< n_- >_{ND}$ = 2.15 and 4.11 respectively.

KNO SCALING

It was concluded a year ago[9] that the KNO scaling limit[10] had already been reached at 50 GeV. Improved data at 102 and 303 GeV and the new data at 405 GeV now indicate that this conclusion may have been precocious. The reduced moments $< n^k > / < n >^k$ and $< n > / D$ have not yet reached their constant asymptotic limits, if indeed they ever will.[11] The empirical observations of Wroblewski seem to give a better description, as can be seen in Figure 11.

Exact KNO scaling may not hold but nevertheless it gives an extremely good parameterization of the data from 20 to 400 GeV.

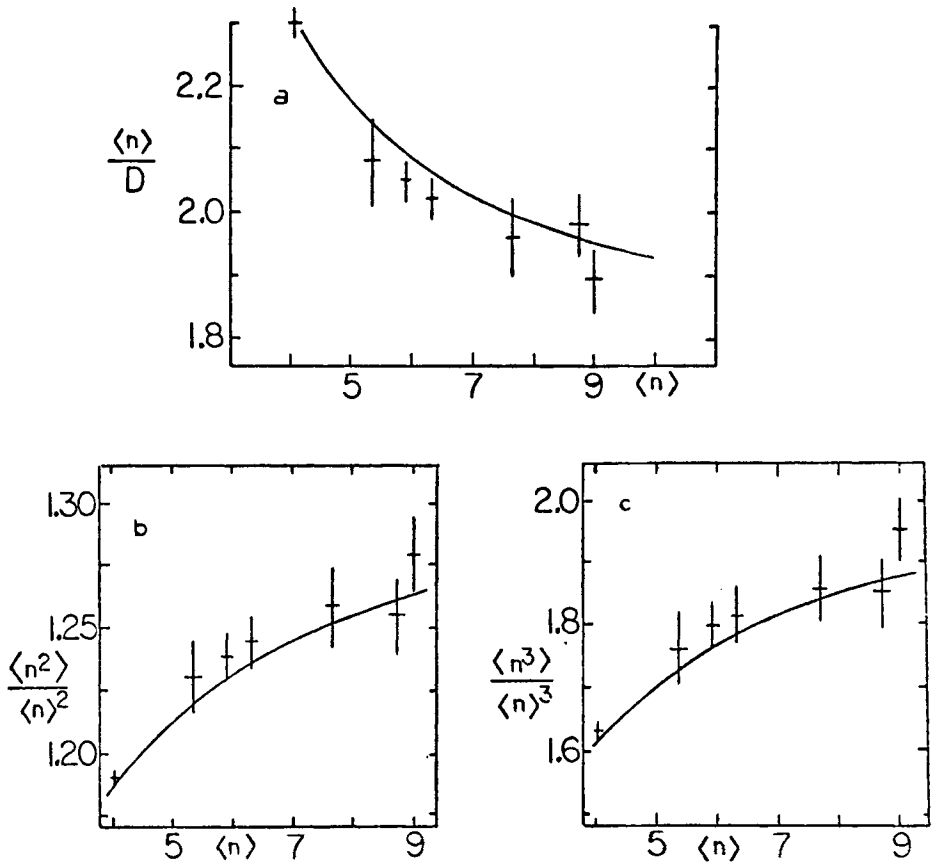

Fig. 11. Various reduced moments vs. $< n >$. Data points are at 19, 50, 69, 102, 205, 303, 405 GeV/c. D is the rms width of the multiplicity distributions. The curves are Wroblewski's parameterizations based on $D = .58\ (< n > -1)$.

III. PRODUCTION OF NEUTRALS

Figure 12 shows the average number of π^o per inelastic collision as a function of ln S. It falls on a straight line (within the large errors) and approximately parallels the $< \pi^- >$ about .4 units higher. NAL points at 100, 200, and 300 GeV are shown.[12,13]

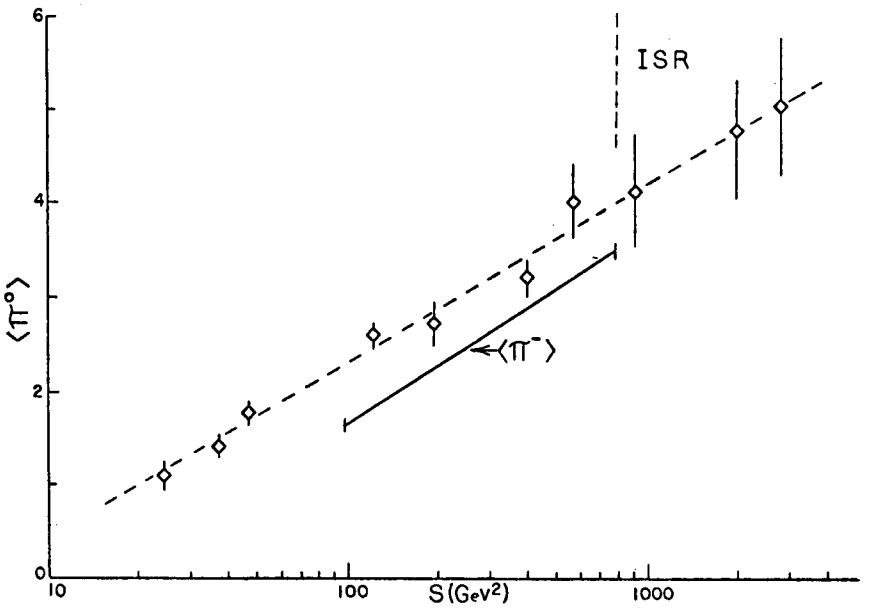

Fig. 12. Average number of π^o per inelastic pp collision. The solid line is a parameterization of $< \pi^- >$ from 50 to 400 GeV/c.

The cross sections as a function of P_{Lab} for K^o, Λ^o, $\bar{\Lambda}^o$ production are shown in Figure 13.[12,13] It appears that the Λ^o cross section may have reached a (temporary ?) plateau above 70 GeV. There appears to be some non-statistical uncertainty associated with these data since cross sections don't always agree at a given energy. It might be wise for the reader to increase all quoted error bars by a factor of two. The production of these neutral strange particles contributes about 5% of the observed π^o production.

The X distributions of these neutral particles at 102 GeV are shown in Figure 14. The γ and K^o data fall off with X in a manner typical of meson production. The Λ^o data peak toward large X indicating the Λ^o are associated with the baryonic charge of the incoming protons. Similar results are found at 69, 205, and 303 GeV.[12,13] The Λ^o show an increase in the fragmentation region above the 24 GeV data of Muck et al.[14]

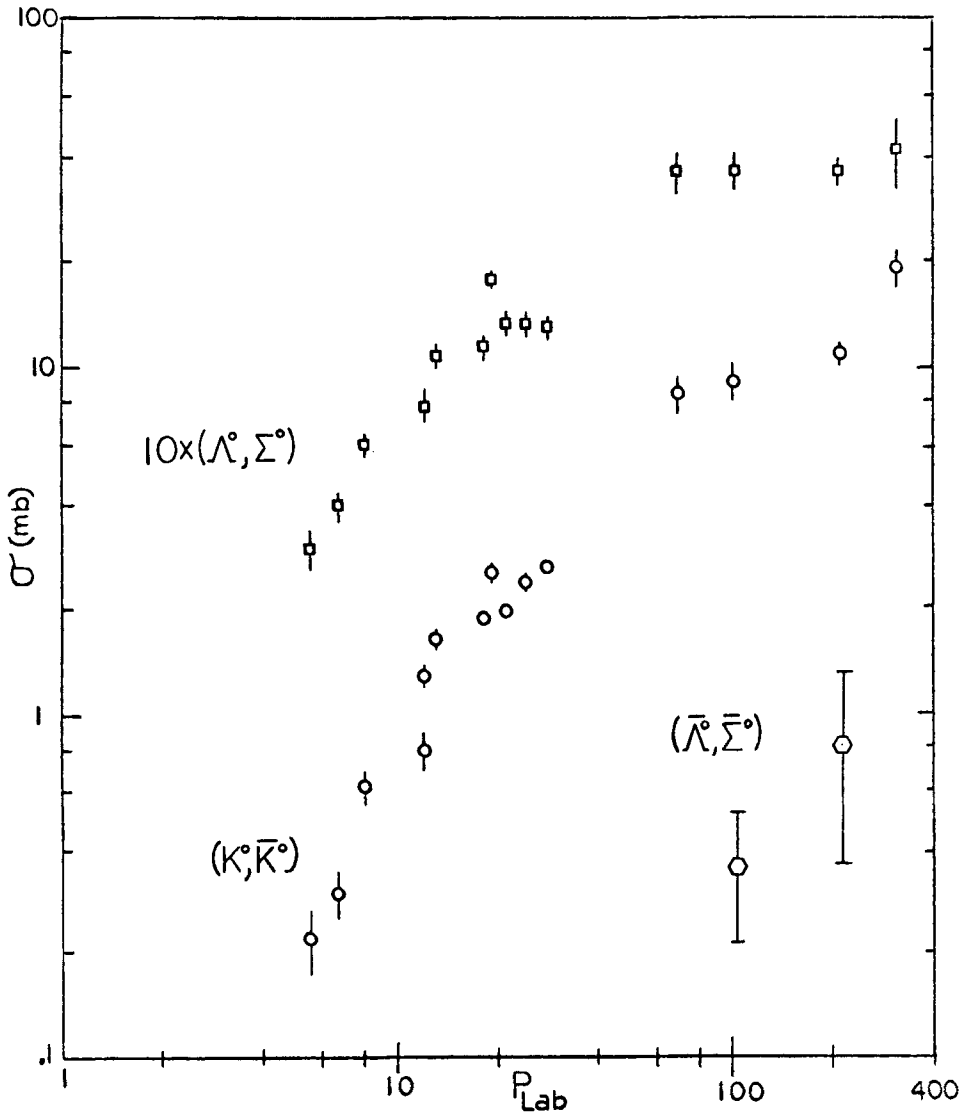

Fig. 13. Inclusive production of neutral strange particles in pp collisions.

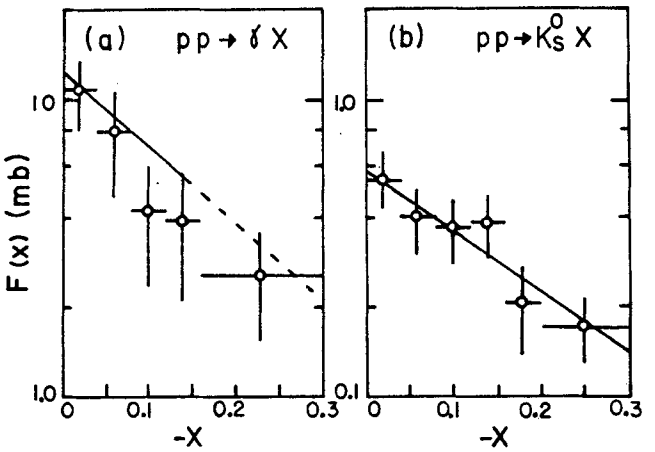

Fig. 14. Invariant cross section integrated over P_T^2 and plotted vs. X. The curves are as follows:

(a) Parameterization of ISR data.

(b) Exp (-4.7 X).

(c) Parameterization of 24 GeV/c data.

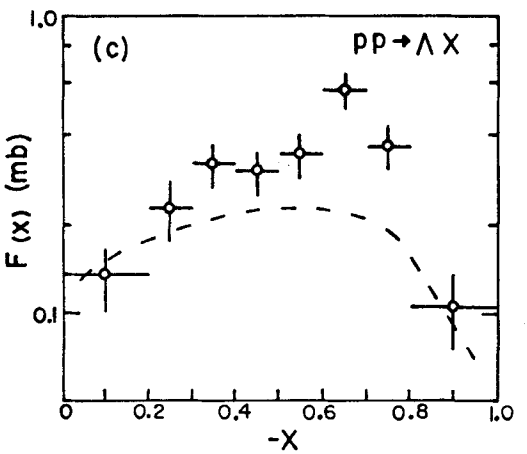

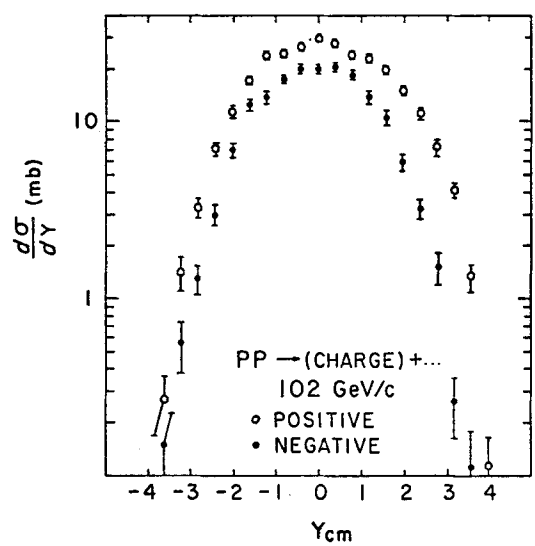

Fig. 15. Inclusive charged particle production at 102 GeV. (Protons have been removed.)

IV. ONE AND TWO PARTICLE INCLUSIVES

Inclusive production of positive (with protons removed) and negative particles at 102 GeV/c is shown as a function of c.m. rapidity in Figure 15. There is a broad central plateau (which is not completely flat). The height of the plateau in fact rises linearly with ln S from 12 to 300 GeV as can be seen in Figure 16.[15]

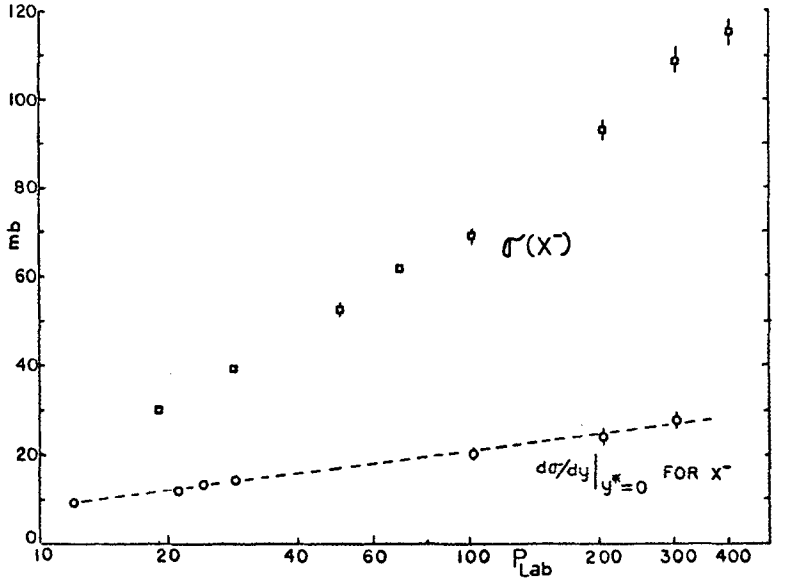

Fig.16. Inclusive negative particle cross section and height of rapidity plateau in pp collisions. Dotted line is (-4.45 + 5.48 ln P) mb.

We see from this that the approximate growth of $\sigma(\pi^-)$ with ln S is <u>not</u> simply due to an energy independent central $d\sigma/dy$ coupled with the simple ln S broadening of the available y range. Life is more complicated than that. The total cross section for making π^- is growing everywhere, except in the fragmentation region tails ($Y_{Lab} \gtrsim 1$).

In the fragmentation region, one-particle inclusive scaling does hold rather well, as can be seen in Figure 17.

This inclusive scaling holds (at least to $\sim \pm$ 10%) all the way up to ISR energies in both $P_{||}$ (Lab) and P_T variables. However, the various topological contributions to the cross section in this region are <u>changing</u> with energy so the picture is not as simple as originally proposed in the limiting fragmentation hypothesis.[16] This topological variation with beam energy is shown in Figure 18 where we have taken a slice ($0 < Y_{Lab} < .5$, corresponding to $0 < P_{||} < \sim .3$ GeV/c) of the data of Figure 17 and plotted the energy variation of its topological components. We see from this that <u>the contributions of the various topologies to the fragmentation region change with energy in a manner very similar to the overall multiplicity cross sections</u>. In this respect there is nothing

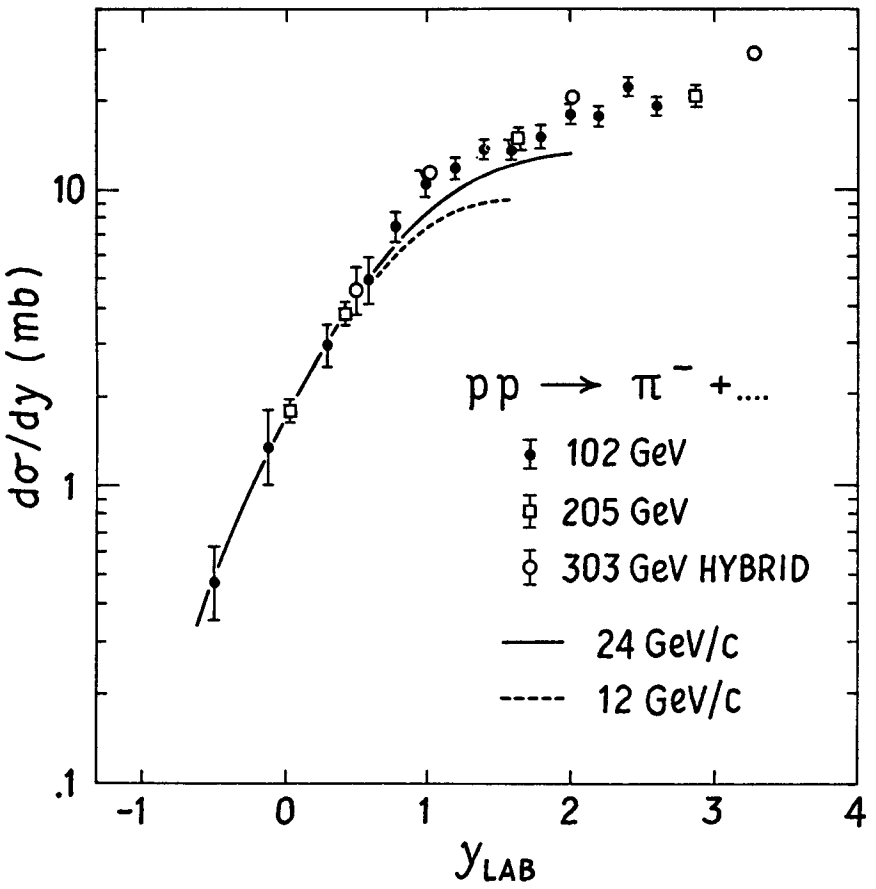

Fig.17. Demonstration of inclusive scaling in the fragmentation region.

special about the fragmentation region. The conspiracy which keeps σ(inelastic) $\approx$ constant while the various σ_n change rapidly apparently operates everywhere.

Turning back to the central region, one can ask how the increase in $d\sigma/dy$ at $y^* = 0$, illustrated in Figure 16, comes about. Does the increase depend on the P_T value in such a way as to give a saturated (or increasing or decreasing) particle density in some invariant momentum space volume elements d^3P/E ? The answer (at least for $P_T \gtrsim 1$ GeV/c) appears to be that the particle density $Ed\sigma/dP^3$ at $y^* = 0$ increases with beam energy by the same proportion at all values of P_T. This is illustrated in Figure 19 which shows invar-

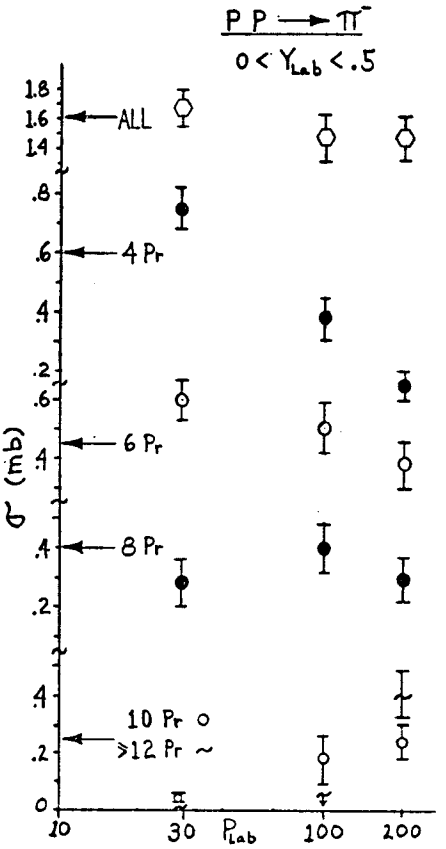

Fig.18. Energy variation of topological contributions to the fragmentation region.

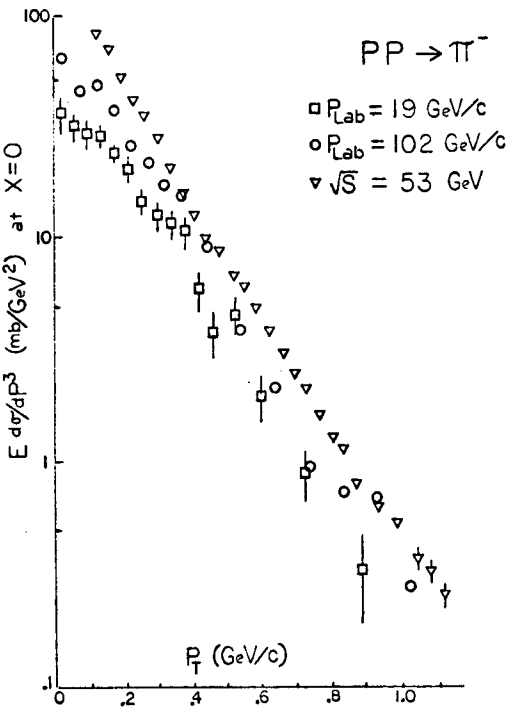

Fig.19. Invariant cross section in the central region vs. P_T for three widely spaced beam energies. Error bars on the 102 GeV/c data are about the same size as on the 19 GeV/c data.

iant cross sections in the central region for $pp \to \pi^-$ at P_{Lab} = 19 GeV/c, 102 GeV/c, and 1500 GeV/c (ISR).[17] The P_T shape is similar at all three energies and appears to level off below $P_T \approx .2$ GeV/c.

CHARGE TRANSFER

It is interesting to see how the particles in individual events distribute themselves in making up the broad rapidity plateau in Figure 15. If we first of all ignore the charges we see that each topology (except 4-prongs) likes to divide its particles evenly between forward and backward hemispheres in the c.m.. This is shown in Figure 20 for the 205 GeV data.

We now look at the amount of charge transfered from one hemisphere to the other (Figure 21). We find that for ≥ 6 prongs it is actually more probable to transfer a single charge than to transfer none. The significant feature of Figure 21 is that the charge transfer frequency for a given topology does not change when the beam energy is doubled.[18] This is certainly not what one expects in any

kind of fragmentation picture. In fact the general features of Figure 21 are fairly well reproduced by putting a nucleon (with probability .5 of being a proton) in each hemisphere and flipping a coin to decide where the remaining pions go!

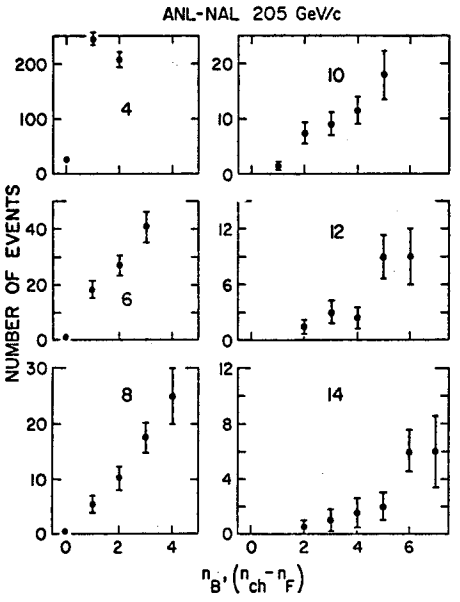

Fig. 20. Frequency of events in a given topology as a function of the number of charged particles in the backward c.m. hemisphere.

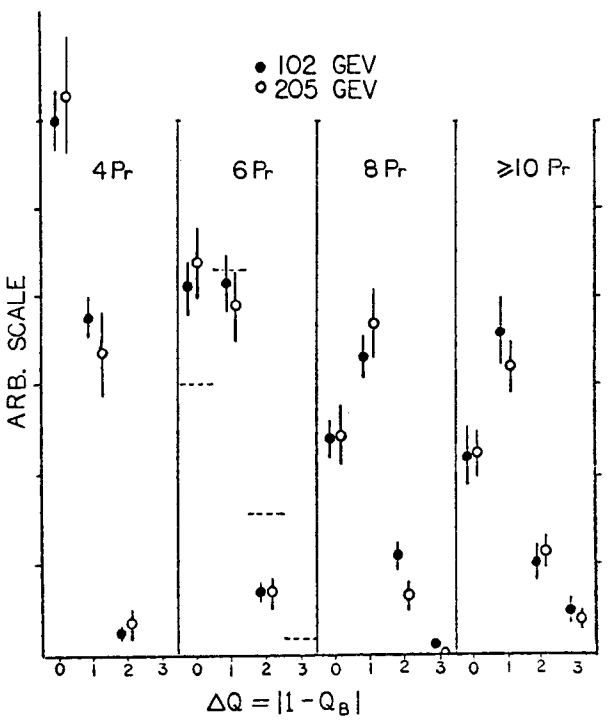

Fig. 21. Charge transfer frequency for various topologies. The dotted line on the 6-prong graph is the result of a penny flipping model.

TWO PARTICLE CORRELATIONS

Good statistics data on two particle correlations are just starting to come out from the NAL bubble chamber.[19] Since the ISR has so far only produced data on charged-charged and charged-neutral correlations it is of interest to see what the individual +-, ++, -- correlations look like. The simplest Mueller-Regge theory predicts no central region correlation for ++ and --.

Looking at the raw two-dimensional distributions $d\sigma/dy_1 dy_2$ is not very enlightening since one sees a broad hump without much structure. This broad hump must be partly due to kinematics and the fact that several entries are made for each event. (A 10-prong gives us 90 entries on the ch-ch plot!) One can be slightly more sophisticated and study the correlation function

$$R_{12} = [\ \sigma(\text{inel})\ d\sigma/dy_1 dy_2\ ]\ [(d\sigma/dy_1)(d\sigma/dy_2)]^{-1} \quad -1$$

for all topologies together. These distributions are also dominated by a broad hump which rises to a height of .4 to .7 in the central region. The only distribution which shows any interesting structure at our present level of statistics and understanding is R_{12} (+-). An example of this is shown in Figure 22 where we see some evidence of a ridge in R_{12} along the line $y_+ = y_-$.

In Table 5 we show the S dependence of R_{12} at $y_1 = y_2 = 0$ in the c.m.. I am told that the fact these heights don't grow ($\propto \sqrt{s}$) is the coup-de-grace for fragmentation-type (e.g. NOVA) models.

Table 5. S Dependence of R_{12}

		Height of R_{12} at $Y_1 = Y_2 = 0$			
P_{Lab}	$\sqrt{s}$	--	++	+-	ch-ch
102	14 GeV	.40	.40	.7	.6
205	20 GeV	~ .3	.35	.7	.6
205 Hybrid	20 GeV	.40			
303 Hybrid	24 GeV	.45			
ISR Pisa - Stony Brook	23-55 GeV				.7

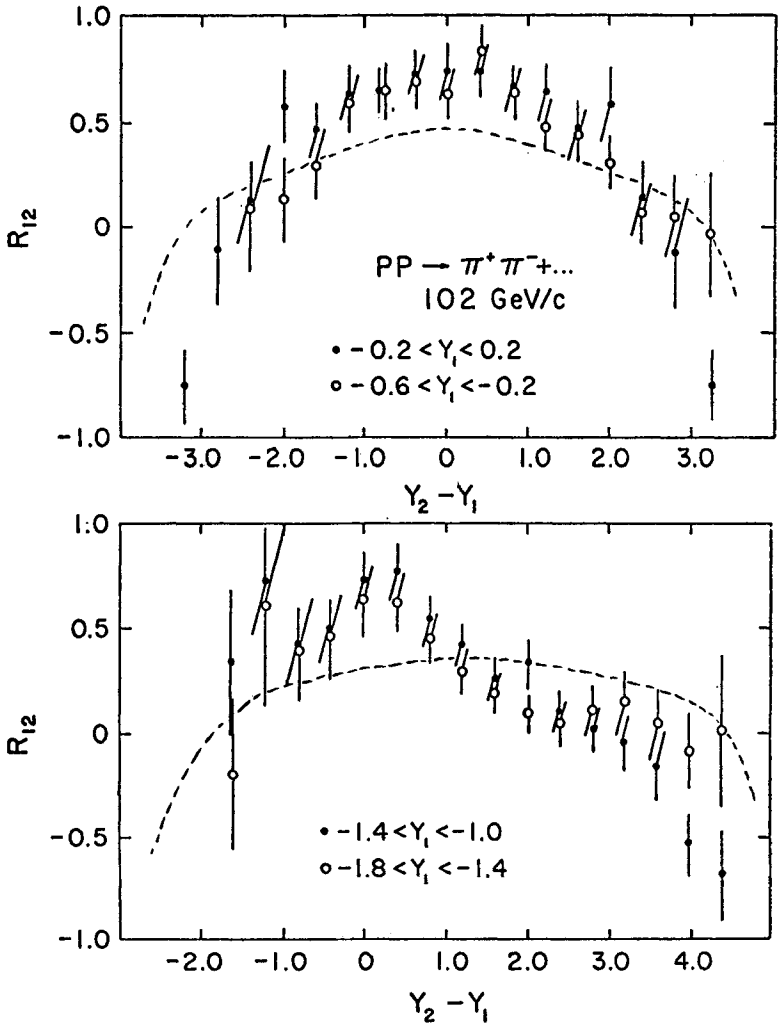

Fig.22. Correlation function for $\pi^+\pi^-$ at 102 GeV. The dotted curves are from a Monte Carlo model of P. Slattery.

Finally let us look at the transverse correlations given by measuring the angle φ between the transverse momentum vectors of two particles. These distributions are shown in Figure 23 for various charge combinations and rapidity separations for the 102 GeV data. The largest back-to-back correlations are seen for +- at small Δy. The ++ and -- data show very little correlation, which may indicate that these particles more frequently have other neutral or charged particles between them in the rapidity chain.

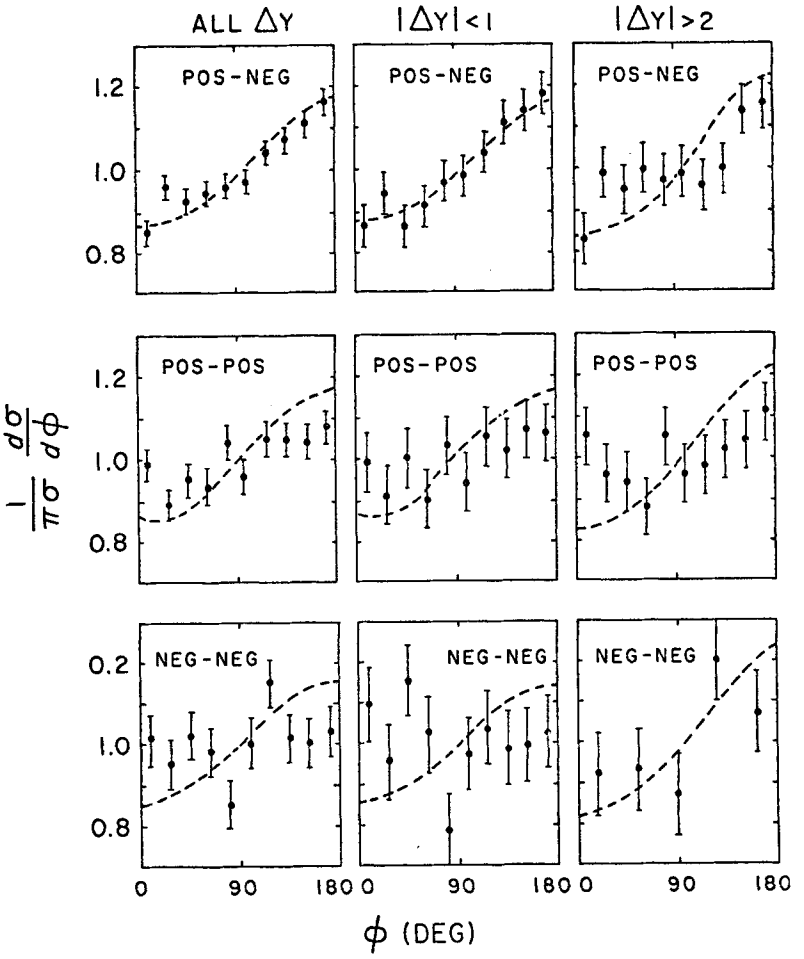

Fig. 23. Transverse correlations at 102 GeV for ≥ 6 prongs with protons removed. The curves are from P. Slattery's Monte Carlo calculation.

Due to transverse momentum conservation there must be a certain amount of back-to-back correlation in the data. It is somewhat surprising that there is in fact so little in the ++ and -- samples.

REFERENCES

(1) J. C. Sens, Proc. of the XVI International Conference on High Energy Physics, Volume 1, 255 (1972).

(2) "Evidence for a Diffractive Component in Multiparticle Production at 102 GeV", Rochester-Michigan preprint UM BC#72-14 UR #416 (1972); J. C. Vander Velde "A Remark about the Fraction of Single Dissociation", Proc. of the XVI International Conference on High Energy Physics, Vol. 1, pp. 260-261 (1972); F. T. Dao et al., "PP Interactions at 303 GeV/c:..." two NAL-UCLA preprints NAL-Pub-73/38-EXP and NAL-Pub-73/22-EXP; S. Barish et al., "PP Interactions at 205 GeV", Argonne-NAL Collaboration, presented by J. Whitmore at the International Conference on High Energy Particle Collisions, Vanderbilt University (Reference 12).

(3) A. Capella et al., Phys. Rev. Letters 31 497 (1973).

(4) M. Derrick et al., Abstract #54, Amer. Phys. Soc. DPF meeting, Berkeley (1973).

(5) J. Whitmore et al., Abstract #48, Amer. Phys.Soc. DPF meeting, Berkeley (1973).

(6) C. Quigg, Rapporteur talk presented at the Amer. Phys. Soc. DPF meeting, Berkeley (1973).

(7) "Evidence for a Diffractive Component in Multiparticle Production at 102 GeV", Michigan-Rochester preprint UMBC 72-14 UR 416 (1972).

(8) F. T. Dao et al., NAL-UCLA preprint NAL-Pub-73/78-EXP UCLA-1077.

(9) P. Slattery, Phys. Rev. Letters, 29 1624 (1972).

(10) Z. Koba, H. B. Nielsen, P. Olesen, Nucl. Phys. B40 317 (1972).

(11) A. Wroblewski, "Remarks on Current Models for Charged Multiplicity Distributions", Warsaw preprint (1972), and Lectures at XIII Cracow School of Theoretical Physics (1973).

(12) Proceedings of the 1973 Vanderbilt Conference, and references given therein. Published by Amer. Inst. of Physics, edited by R. S. Panvini.

(13) G. Charlton et al., Phys. Rev. Letters 29 1759 (1972)
G. Charlton et al., Phys. Rev. Letters 30 574 (1973)
F. T. Dao et al., Phys. Rev. Letters 30 1151 (1973)
J. W. Chapman et al., Michigan-Rochester preprint (1973) (To be published).
K. Jaeger et al., ANL Preprint, Abstract 53, Berkeley D.P.F. meeting (1973).

(14) H.J. Muck et al., DESY report F1-72/1 (1972).

(15) Data for Figure 16, 17 and 18 were extracted from : H. J. Muck et al., Phys. Letters 39B 303 (1973); W. H. Sims et al., Nucl. Phys. B41 317 (1972); E. L. Berger et al., ANL preprint ANL/HEP 7209 (1972); G. Smith et al., NAL HYBRID Experiment 2B, Abstract 38, Berkeley D. P. F. meeting (1973); Michigan-Rochester preprint UMBC 73-19 UR-460 (1973); J. Whitmore, private communication. See also reference 20.

(16) J. Benecke et al., Phys. Rev. 188 2159 (1969).

(17) 19 GeV/c data from H. Boggild (private communication); 102 GeV/c data from the Michigan-Rochester Collaboration; 1500 GeV/c data from the British-Scandanavian Group (ISR).
(18) The 205 GeV charge transfer results were provided to us by R. Englemann, private communication.
(19) 102 GeV data: C. Bromberg et al., to be published.
205 GeV data: R. Englemann et al., Abstract 47, Berkeley, D. P. F. meeting (1973).
205 and 303 GeV Hybrid data: G. Smith et al., ref. 15.
(20) The data we use for charged particle multiplicites in pp collisions can be found in the following references:
19 GeV/c: H. Boggild et al., Nuclear Phys. B27 285 (1971).
28.5 GeV/c: W. H. Sims et al., ref. 15.
50 and 69 GeV/c: V. V. Ammosov et al., Phys. Letters 42B 519 (1972).
102 and 405 GeV/c: Michigan-Rochester preprint UMBC 73-18 UR 459 (to be published).
205 GeV/c: G. Charlton et al., Phys. Rev. Letters 29 515 (1972) and J. Whitmore, ref. 12.
303 GeV/c: F. T. Dao et al., NAL-UCLA preprint NAL 73/38 UCLA-1077.

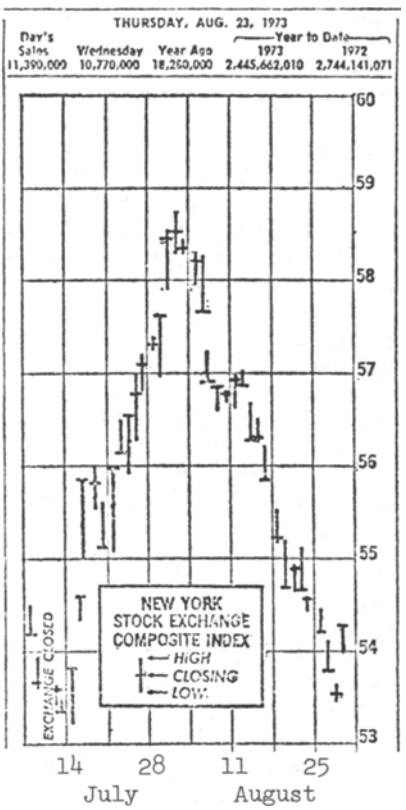

Fig. 562.

Time-dependent $-$ correlation function from the NYSE collaboration.